

Figure. 1 X-ray powder diffractogram of rGO/Bi.

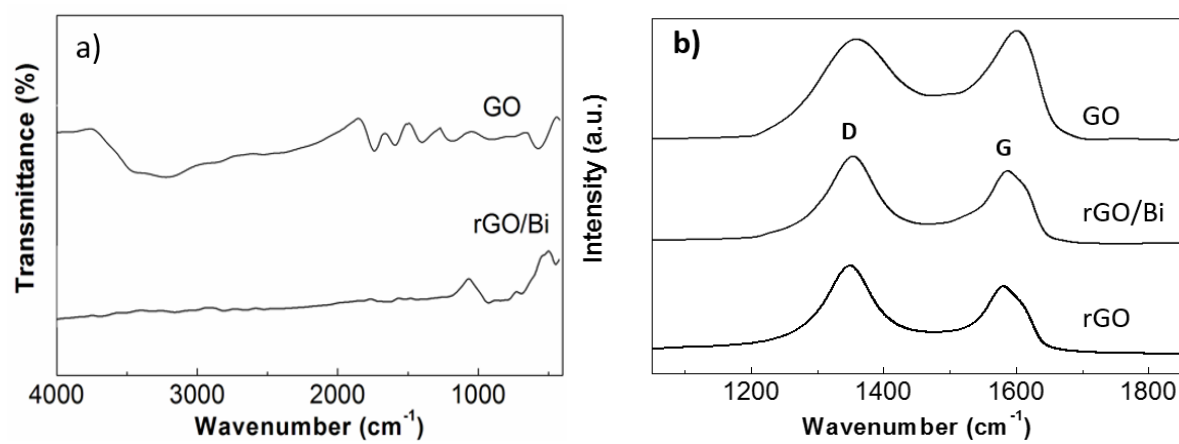


Figure 2. a) FTIR spectra of GO and rGO/Bi b) Raman spectra of GO, rGO/Bi and rGO.

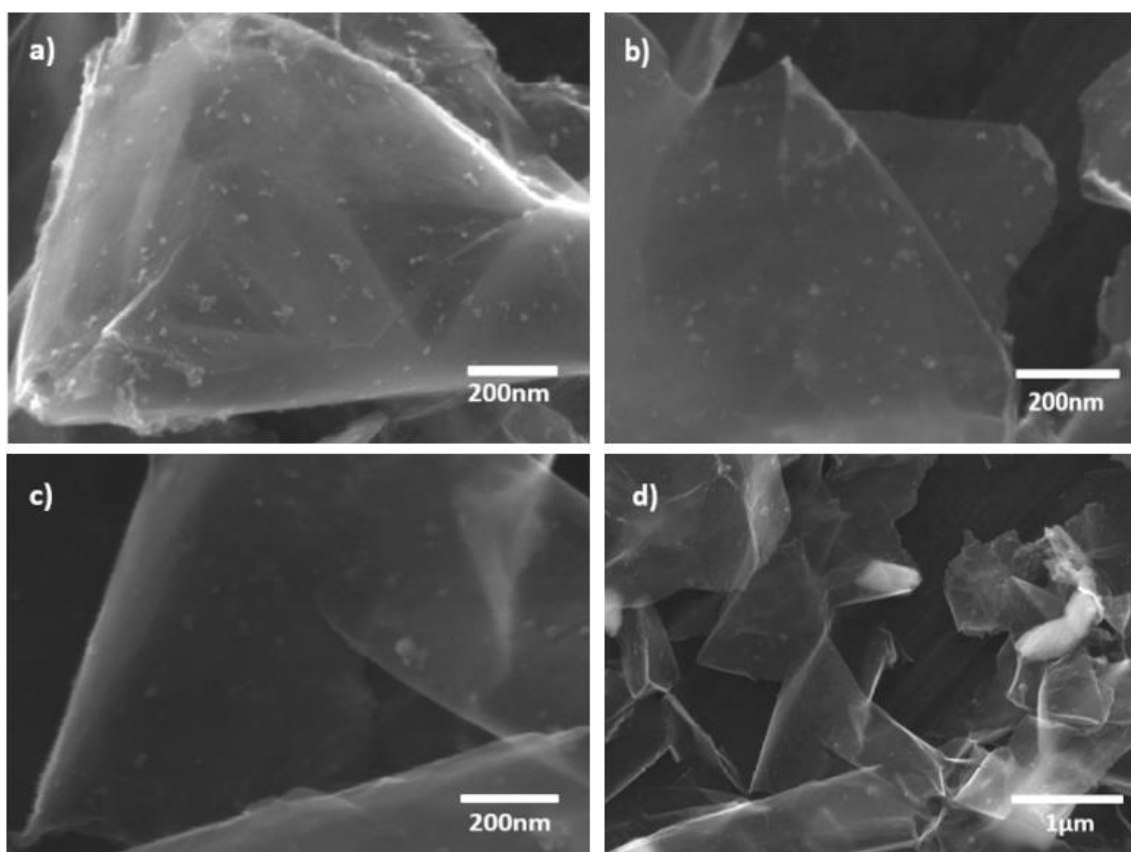


Figure 3. SEM images of the as prepared rGO/Bi composite at a) 80,000x, b) 100,000x, c) 100, 000x and d) 25, 000x magnification.

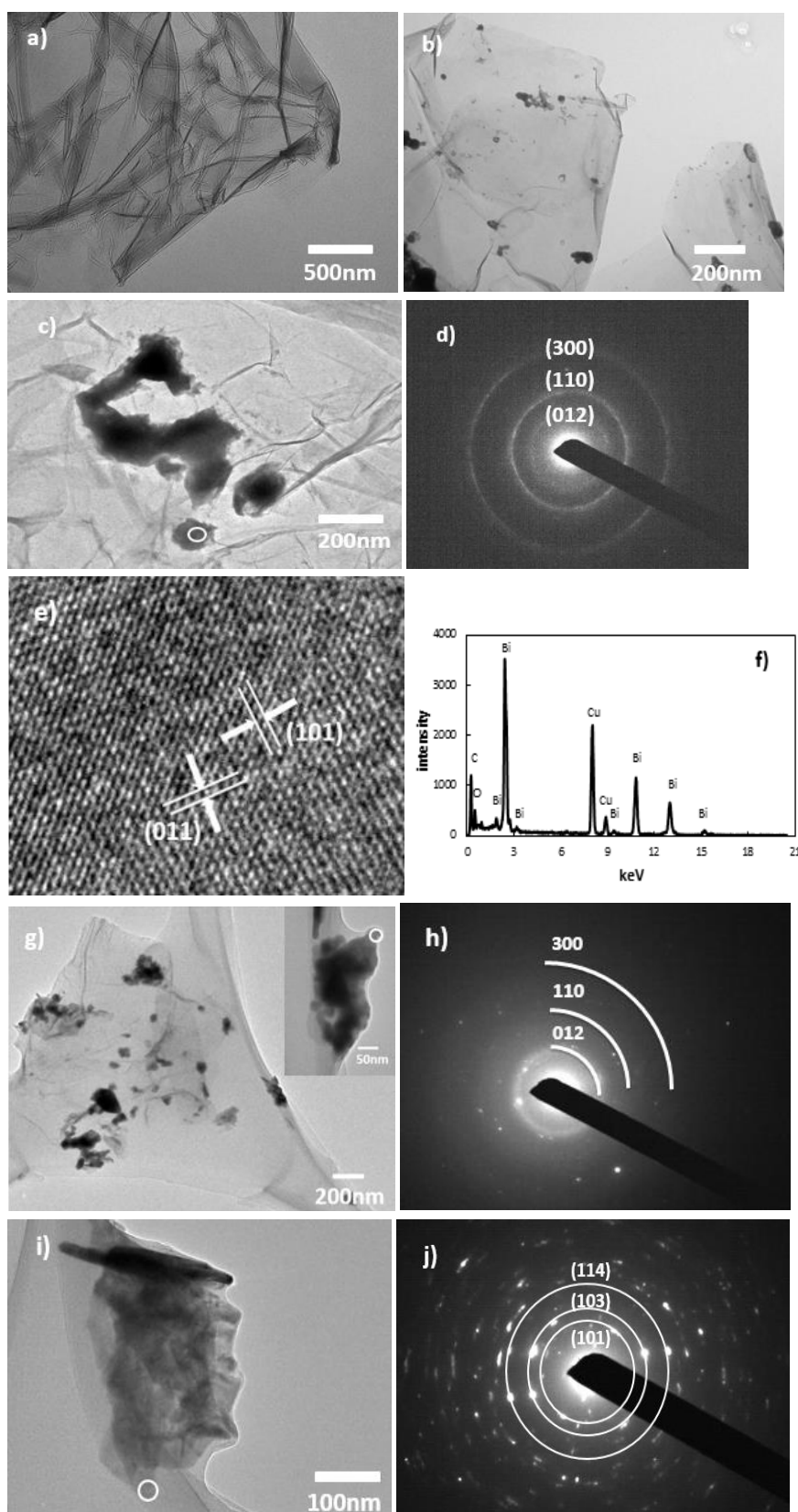


Figure 4. a) TEM image of rGO; b) TEM image of as-prepared rGO/Bi; c) TEM image of rGO/Bi showing a region containing Bi agglomerates; d) selected area electron diffraction (SAED) measured on rGO/Bi; e) crystalline structure observed by HRTEM in as-prepared rGO/Bi; f) EDS from as-prepared rGO/Bi; g) TEM image of rGO/Bi after electrochemical cycling; h) selected area electron diffraction (SAED) after electrochemical cycling showing the presence of metallic Bi; i) TEM images of rGO/Bi after electrochemical cycling; j) selected area electron diffraction (SAED) after electrochemical cycling, showing the presence of bismuth subcarbonate.

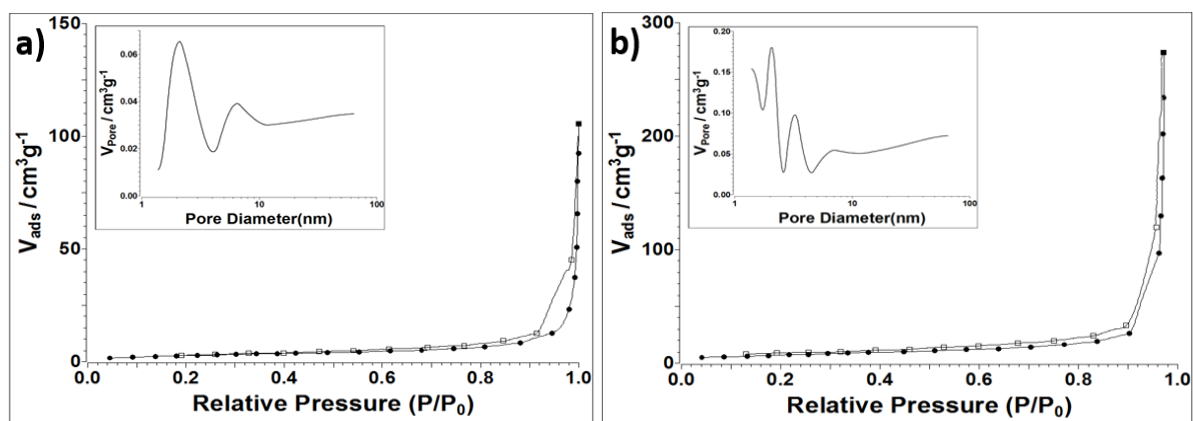


Figure 5 Nitrogen adsorption-desorption isotherms of a) rGO/Bi b) rGO.

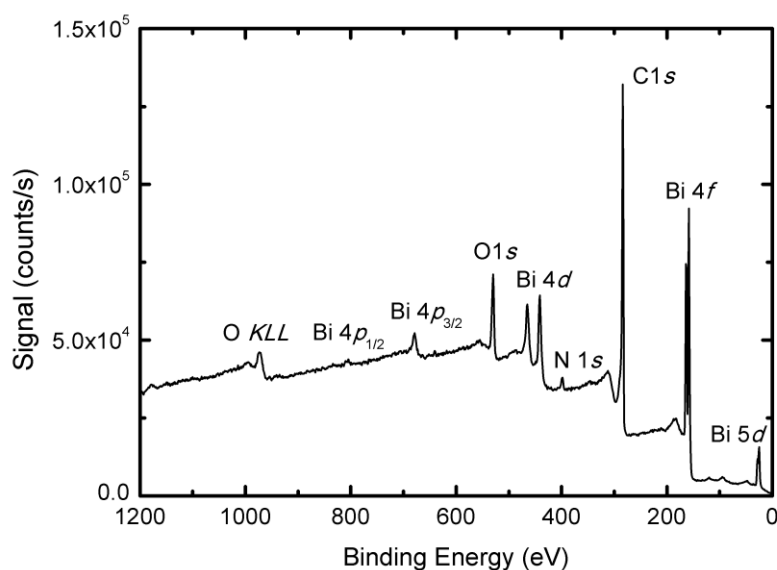


Figure 6. XP survey spectrum obtained from 27 month-old rGO/Bi composite.

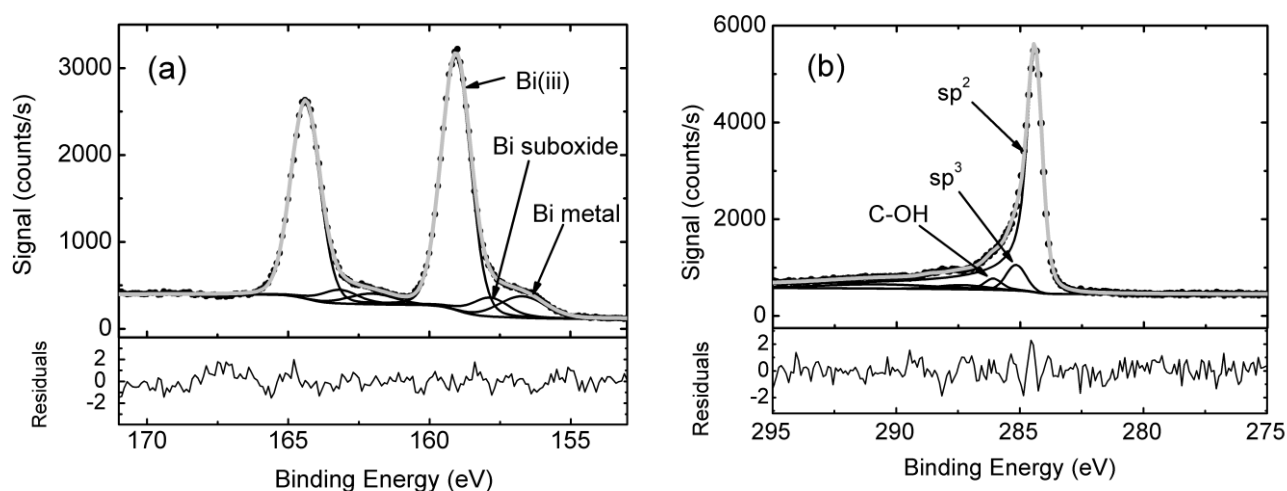


Figure 7. a) Top panel: Bi $4f$  XP spectrum of the rGO/Bi composite and associated fit. The Bi  $4f_{7/2}$  components are associated with metallic Bi, Bi suboxide and Bi in the +3 oxidation state (Bi(iii)). Bottom panel: Fit residuals in units of standard deviation of the data. b) Top panel: C $1s$  XP spectrum of the rGO/Bi composite and associated fit. The three largest fit components, associated with  $sp^2$ ,  $sp^3$  carbon and C-OH are labelled. Bottom panel: Fit residuals in units of standard deviation of the data. In both spectra black dots represent the experimental data, the grey line the fit to the spectrum and the black lines the individual fit components and Shirley background.

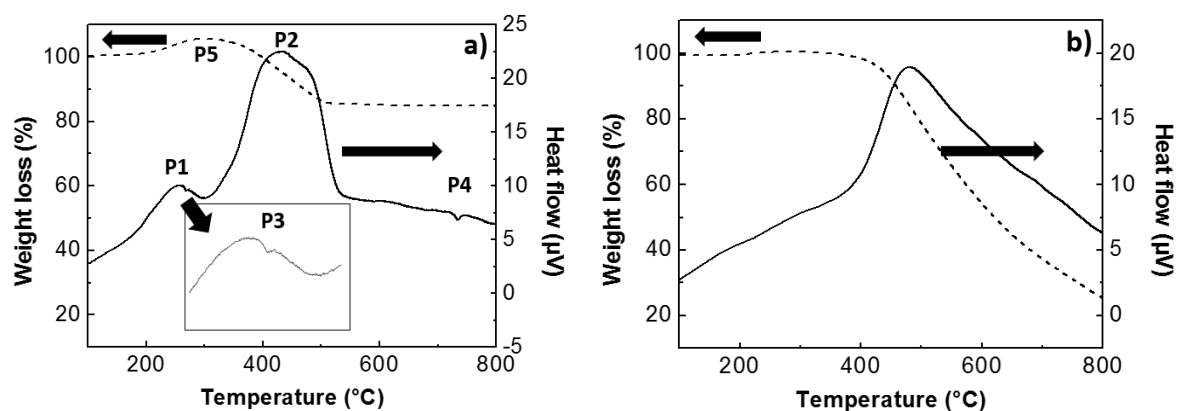


Figure 8. DTA and TGA curves of a) rGO/Bi b) rGO.

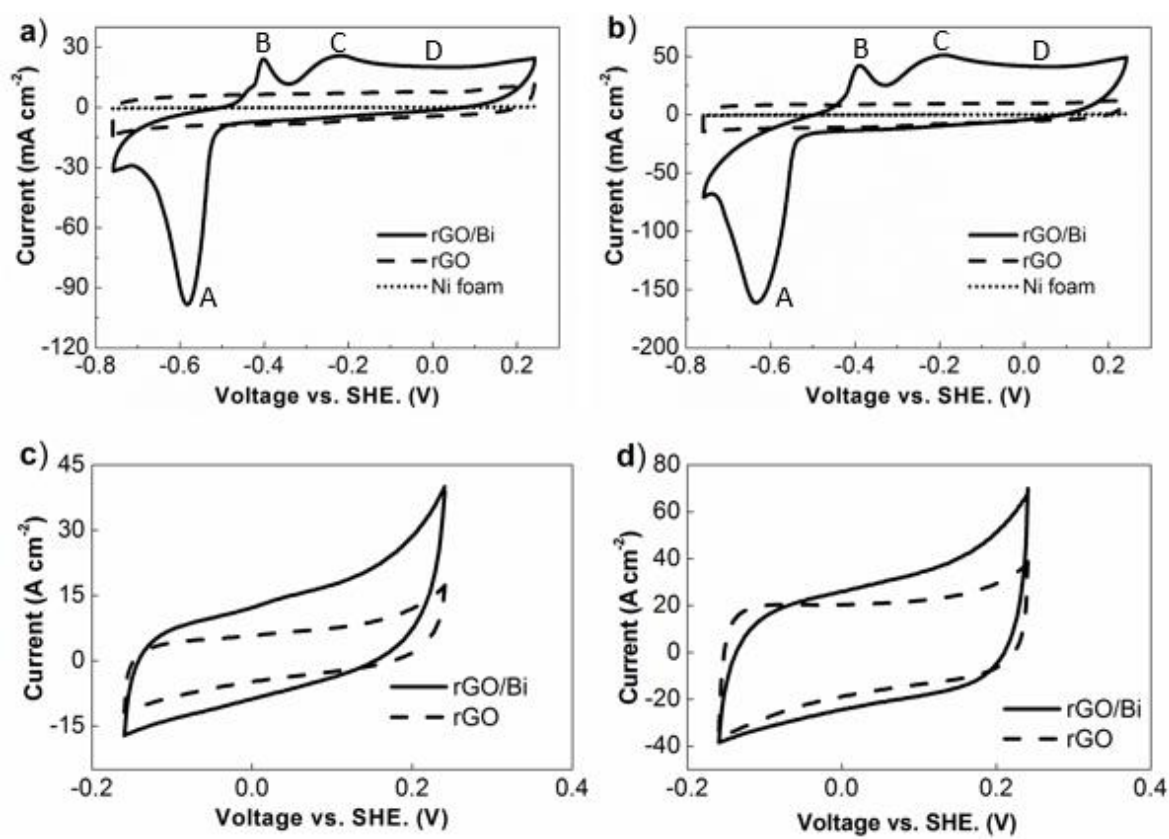


Figure 9. Typical CV results of rGO/Bi, rGO and Ni foam within different voltage range at scan rates of a)  $20\text{mV s}^{-1}$  b)  $50\text{mV s}^{-1}$  c)  $20\text{mV s}^{-1}$  d)  $50\text{mV s}^{-1}$ .

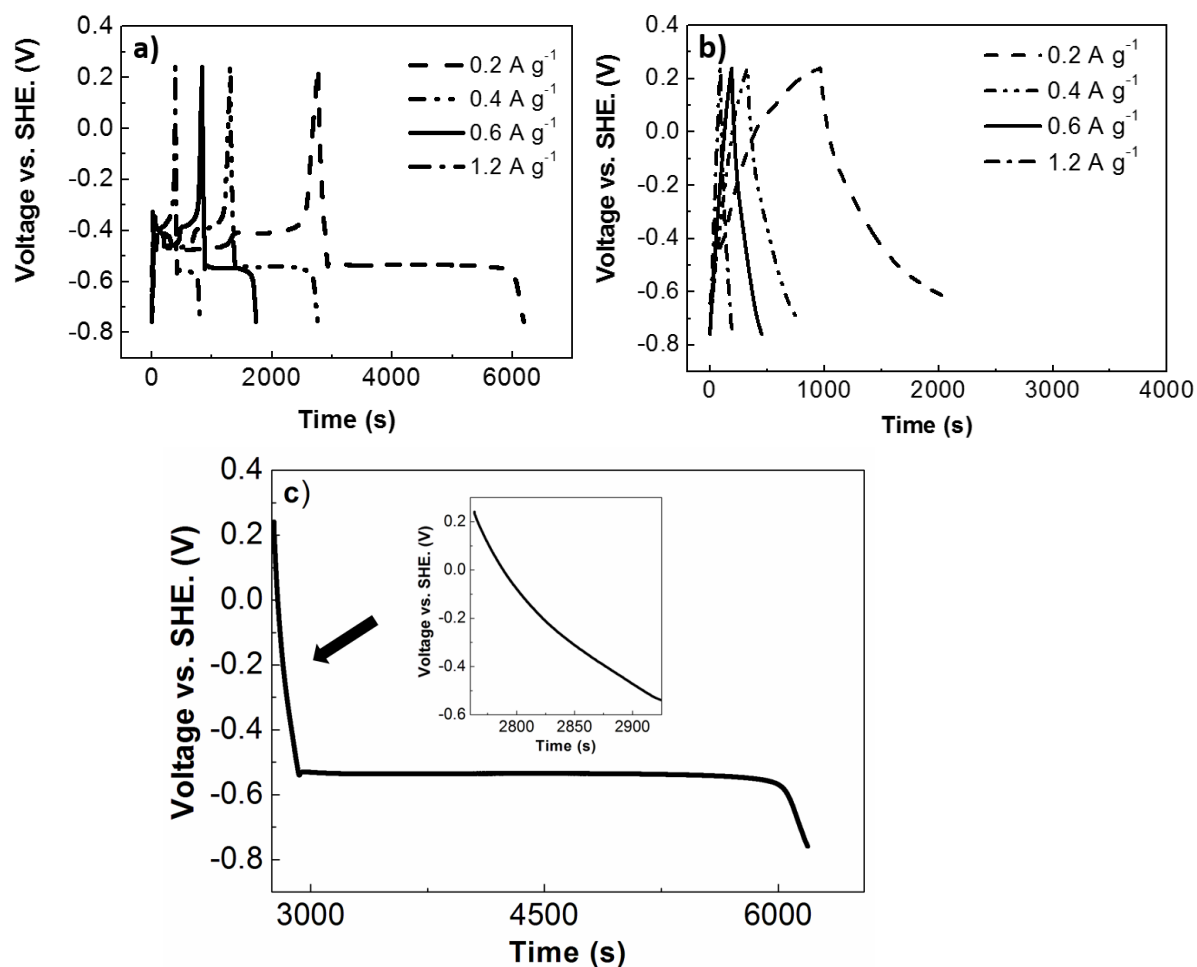


Figure 10. Typical charge/discharge behaviours of a) rGO/Bi at different current densities b) rGO at different current densities c) enlarged discharge curve of rGO/Bi at 0.2 A g<sup>-1</sup>.

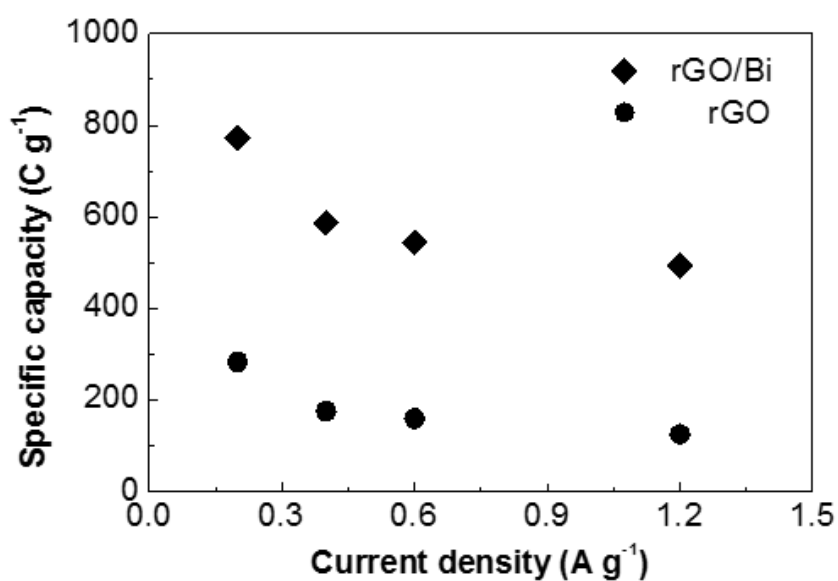


Figure 11. Specific capacity of rGO/Bi and rGO calculated from charge/discharge curves.

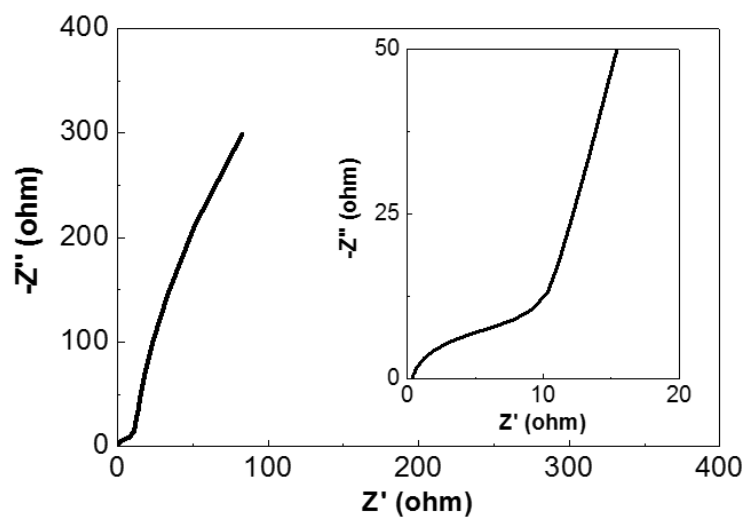


Figure 12. Nyquist plot for the rGO/Bi composite. The inset provides an enlarged view of the high frequency region.

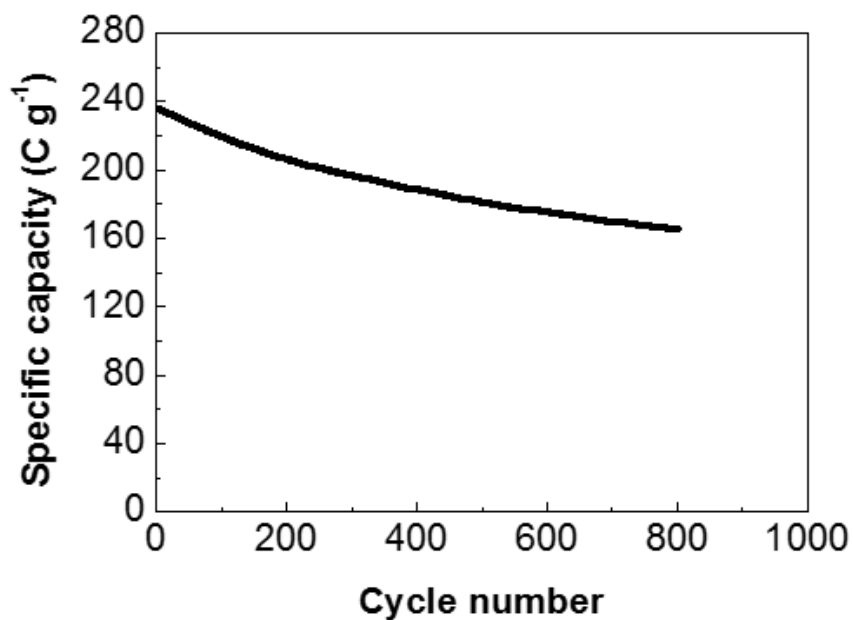


Figure 13. Life-cycle test of rGO/Bi composite under  $5 \text{ A g}^{-1}$  current density.